Global coseismic deformations, GNSS time series analysis, and earthquake scaling laws

Laurent Métivier, Xavier Collilieux, Daphné Lercier, Zuheir Altamimi, François Beauducel

AGU PUBLICATIONS

JGR

Journal of Geophysical Research: Solid Earth

RESEARCH ARTICLE
10.1002/2014JB011280

Key Points:
- Global modeling of coseismic deformations during two decades
- Improved detection of discontinuities in GPS time series induced by seismicity
- Consistency between earthquake scaling laws and geodetic observations

Supporting Information:
- Readme
- Table S1
- Figure S1

Correspondence to:
L. Métivier,
laurent.metivier@ign.fr

Citation:
Métivier, L., X. Collilieux, D. Lercier, Z. Altamimi, and F. Beauducel (2014), Global coseismic deformations, GNSS time series analysis, and earthquake scaling laws, *J. Geophys. Res. Solid Earth*, *119*, 9095–9109, doi:10.1002/2014JB011280.

Received 14 MAY 2014
Accepted 29 OCT 2014
Accepted article online 5 NOV 2014
Published online 4 DEC 2014

Global coseismic deformations, GNSS time series analysis, and earthquake scaling laws

Laurent Métivier[1], Xavier Collilieux[1], Daphné Lercier[1], Zuheir Altamimi[1], and François Beauducel[2]

[1]IGN LAREG, Université Paris Diderot, Sorbonne Paris Cité, Paris CEDEX 13, France, [2]Institut de Physique du Globe de Paris, Sorbonne Paris Cité, CNRS UMR7154, Paris, France

Abstract We investigate how two decades of coseismic deformations affect time series of GPS station coordinates (Global Navigation Satellite System) and what constraints geodetic observations give on earthquake scaling laws. We developed a simple but rapid model for coseismic deformations, assuming different earthquake scaling relations, that we systematically applied on earthquakes with magnitude larger than 4. We found that coseismic displacements accumulated during the last two decades can be larger than 10 m locally and that the cumulative displacement is not only due to large earthquakes but also to the accumulation of many small motions induced by smaller earthquakes. Then, investigating a global network of GPS stations, we demonstrate that a systematic global modeling of coseismic deformations helps greatly to detect discontinuities in GPS coordinate time series, which are still today one of the major sources of error in terrestrial reference frame construction (e.g., the International Terrestrial Reference Frame). We show that numerous discontinuities induced by earthquakes are too small to be visually detected because of seasonal variations and GPS noise that disturb their identification. However, not taking these discontinuities into account has a large impact on the station velocity estimation, considering today's precision requirements. Finally, six groups of earthquake scaling laws were tested. Comparisons with our GPS time series analysis on dedicated earthquakes give insights on the consistency of these scaling laws with geodetic observations and Okada coseismic approach.

1. Introduction

The stress accumulation induced by plate tectonics usually releases in earthquake (EQ) ruptures along faults close to plate boundaries or within deforming regions. EQs induce coseismic deformations in the crust and may generate large abrupt changes in the position of geodetic stations, which are particularly visible in Global Navigation Satellite System (GNSS) position time series, in particular Global Positioning System (GPS). Coseismic deformations have been investigated for many years with geodetic techniques, particularly for selected EQs of interest [e.g., *Fialko et al*., 2001; *Subarya et al*., 2006; *Shestakov et al*., 2012]. The detection of far-field coseismic displacements caused by the Sumatra–Andaman EQ [e.g., *Vigny et al*., 2005; *Fu and Sun*, 2006; *Kreemer et al*., 2006], for instance, showed the power of using GPS estimates to quantify global deformation. More generally, *Tregoning et al*. [2013] showed that EQs with magnitude larger than 8 significantly impact the position of GPS stations thousands of kilometers away from the EQ epicenters, considering the precision of measurement of GPS today, which is at the level of a few millimeters.

In the present work, we address the question of the global impact of coseismic deformations, from all types of EQs, on geodetic measurements and on the International Terrestrial Reference Frame (ITRF) elaboration. In return, we investigate what information a global GPS homogeneous data set gives on EQ parameter scaling relations considering the approach that we use.

The ITRF solutions are presently published as reference tables of positions and long-term linear velocities for a set of globally distributed geodetic stations, which are updated every 3–5 years in order to comply as much as possible with the International Terrestrial Reference System specifications. The ITRF is classically constructed by a combination of station position time series provided by the four space geodetic techniques: GNSS, very long baseline interferometry, satellite laser ranging, and Doppler orbitography and radiopositioning integrated by satellite. Coordinates in these tables are supplied as piecewise linear functions of time [e.g., *Altamimi et al*., 2002, 2007, 2011]. The main linear component of the ITRF coordinates is largely due to plate tectonics [*Altamimi et al*., 2012] in the horizontal components. However, it is well known that station positions also exhibit nonlinear behaviors due to various geophysical phenomena and

systematic technical errors [*Dong et al*., 2002; *Collilieux et al*., 2007; *Ray et al*., 2008; *Métivier et al*., 2012]. When Earth deformation models are available with sufficient accuracy like for solid Earth tides (see the discussion in *Métivier et al*. [2005, 2006, 2007] and *Métivier and Conrad* [2008]), pole tides, or the ocean tidal loading, they are used to correct geodetic observations and so are no longer delivered in ITRF coordinates. EQs also induce nonlinear changes in station positions. Currently, the EQ effects are partially modeled in ITRF coordinates through coordinate discontinuities and velocity changes. Those discontinuities in station position time series are usually detected by visual inspection, but such analysis is very fastidious and strongly depends on the operator. Moreover, the presence of a misplaced or undetected offset generally strongly impacts the velocity estimations. The problem is particularly important in GNSS analysis due to the density of GPS stations in EQ-impacted areas and due to GPS precision. Considering that the scientific community requires a terrestrial reference frame that is accurate and stable at the level of 1 mm and 0.1 mm/yr in its defining parameters and their time evolutions, respectively [*Plag and Pearlman*, 2009], a great effort has to be made to reduce errors in position time series and station velocity determinations, which calls for more investigation on the treatment of discontinuities in geodetic time series. A few approaches have been proposed for automated detection of discontinuities in GNSS time series based on various statistical methods [*Williams*, 2003; *Perfetti*, 2006; *Vitti*, 2012; *Gazeaux et al*., 2013]. Unfortunately, up to now, automated methods do not give better results than the classical manual method [*Gazeaux et al*., 2013].

Discontinuities are typically due to equipment changes or malfunctions, EQ ruptures, or changes in the environment of the stations. We propose to investigate here offsets related to EQs. Based on geophysical modeling, we develop a method to predict the effect of coseismic deformations on position series (section 2). We show here that intermediate EQs (magnitudes 6 to 8) can also have a significant impact on GPS station displacements. In section 3, we apply our method on coordinates of a global GPS network in order to improve the detection of discontinuities in position time series. We study and outline the interest to rely on such a prediction process for determining station long-term velocities and, therefore, for the construction of a terrestrial reference frame. Our aim is not to propose a general method for discontinuity detection in GPS time series. We only focus on the particular case of EQ-related discontinuities. We aim to show that simple coseismic modeling assumptions combined with geophysical information allow to detect many small discontinuities that are usually missed. Such information could be used as a priori information in a more general automated method for change point detection in GPS time series. As a by-product of this work, we plan to set up a Web service that will provide coseismic offsets on demand for a list of stations that would be given by the Web user. Finally, in section 4, the predicted coseismic displacements are compared to the amplitudes of the estimated offsets in GPS time series. We take the example of the Hector Mine EQ and study global EQ scaling laws with respect to GPS observations.

2. Theoretical Coseismic Displacements

2.1. Modeling of Deformation

Every EQ generates coseismic deformations in a region surrounding its epicenter with various geographical extents and patterns [e.g., *Aki and Richards*, 1980]. A perfect modeling of coseismic deformations would be extremely complex because it would strongly depend on the local topographical and geological characteristics of the region. The present work aims at globally evaluating the impact of coseismic deformations during a given period. For this reason, we choose here to model coseismic deformations with a general simple method that may be less precise than a local numerical model but offers the benefit of rapidity and nevertheless gives realistic geographical patterns and correct orders of magnitude. We used the so-called Okada approach [*Okada*, 1985], which provides analytical solutions for deformations due to shear and tensile faults in an elastic half space.

We investigate here 20 years of theoretical global surface deformations induced by successive EQs using a U.S. Geological Survey (USGS) National Earthquake Information Center (NEIC) catalog of seismic source parameters (provided by the global centroid moment tensor (CMT) project [*Dziewonski et al*., 1981; *Ekström et al*., 2012]). The catalog provides a list of worldwide EQs containing more than 25,000 events from 1977 to 2010, with their magnitude (larger than 4 but probably complete only for magnitude larger than 5.5), epicenter locations, principal axes, and nodal plane characteristics. The catalog is no longer provided by the USGS NEIC, but an updated version can be found on the CMT website. We calculated the coseismic ground deformations due to all the EQs. Considering that we did not know which nodal plane corresponds to the actual fault plane, we calculated the solution for both nodal planes for each EQ.

Table 1. The Different Published Statistics That we Used as Earthquake (EQ) Scaling Laws With a Few Details on the EQ Database Investigated by the Authors

Acronym	EQ Scaling Model	Comments
WC94	*Wells and Coppersmith* [1994]	All type of EQs; worldwide
MB00	*Mai and Beroza* [2000]	All type of EQs; worldwide
BL10	*Blaser et al.* [2010]	All type of EQs; worldwide
ST10	*Strasser et al.* [2010]	Subduction zone EQ; worldwide
YM11a	*Yen and Ma* [2011]	All type of EQs; mostly Taiwan orogenic belt
YM11b	*Yen and Ma* [2011]; moment threshold	Same database but two distinct scaling regimes depending on EQ moment

However, the EQ catalog does not provide all the necessary information for applying the Okada approach. Indeed, the length and the width of the fault plane need to be known as well as the magnitude of the EQ slip. We therefore investigated different published EQ scaling statistics to determine those values from EQ magnitude or moment magnitude. EQs are generally thought to follow self-similar scaling, in which the source dimensions are scale invariant [*Scholz*, 1990; *Mai and Beroza*, 2000]. Based on source parameter compilations of historical EQs and local observations, many studies propose global scaling laws that link the EQ magnitude, the fault surface dimension, and the fault slip. These scaling laws typically assume linear relations between the EQ magnitude and the logarithm of the different fault rupture parameters such as

$$\log P = a\ M + b \tag{1}$$

where P denotes a given fault parameter, M is the EQ magnitude, and a and b are real constants. P here may be the mean width or the mean length of the rupture area or the average fault slip. Table 1 gives the different statistics that we used in the present work with a few details on the EQ database that has been investigated by the authors who inferred the statistics. The *Wells and Coppersmith*'s [1994] scaling relations are among the most widely used in seismology, but many authors have compiled more recent scaling laws using different or larger databases. In addition to *Wells and Coppersmith* [1994], we investigated scaling relations from *Mai and Beroza* [2000], *Blaser et al*. [2010], *Strasser et al*. [2010], and finally two groups of scaling laws from *Yen and Ma* [2011]. The second group of laws from *Yen and Ma* [2011] is by itself composed of two groups of scaling laws, one dedicated to EQs with moment magnitude larger than 10^{20} Nm (EQ magnitude approximately equal to 7.3) and the other to EQs with moment magnitude smaller. The aim of the present paper is not to investigate all the published scaling relations but rather to see if different scaling laws significantly impact our results. Many other studies have been published on the subject of scaling laws, for example, by *Murotani et al*. [2008] or *Romanowicz and Ruff* [2002].

Note that observations and definitions of the fault lengths and widths may be different in the different studies. *Wells and Coppersmith* [1994], for example, determine fault rupture dimensions from the spatial extent of early aftershocks, while *Mai and Beroza* [2000], *Strasser et al*. [2010], and *Yen and Ma* [2011] determine the fault parameters from finite fault rupture models derived from inversion of strong motion recording and/or geodetic observations [e.g., *Freymueller et al*., 1994; *Peltzer et al*., 2001; *Ji et al*., 2002; *Jacobs et al*., 2002; *Simons et al*., 2002; *Hreinsdottir et al*., 2003; *Salichon et al*., 2004]. As a consequence, the geometrical quantities derived from finite fault models are only effective parameters that may be different to what is really observed in the field but that are believed to better contribute to explain the deformation observations [*Mai and Beroza*, 2000]. Finally, *Blaser et al*. [2010] compile many published observations, including *Wells and Coppersmith*'s [1994] and *Mai and Beroza*'s [2000] fault parameter databases, which are, as we mentioned before, quite different in nature.

It is worth mentioning that the fault models that can be inferred from these statistics are very simple. It is well known, for instance, that fault slips, in reality, are spatially variable along fault ruptures. In addition, we assume here that the fault brakes uniformly around the epicenter, while it is well known that EQ rupture sometimes propagates unilaterally. We also note that some EQ hypocenters, particularly for small teleseismic EQs, may not be precisely determined. Finally, we calculated the global coseismic deformation induced by an EQ with a method that assumes an infinite half space around the epicenter. All these issues may affect the accuracy of coseismic deformation determinations. But we must insist here that we do not aim to develop a precise method for coseismic deformation calculations but investigate if simple methods help to

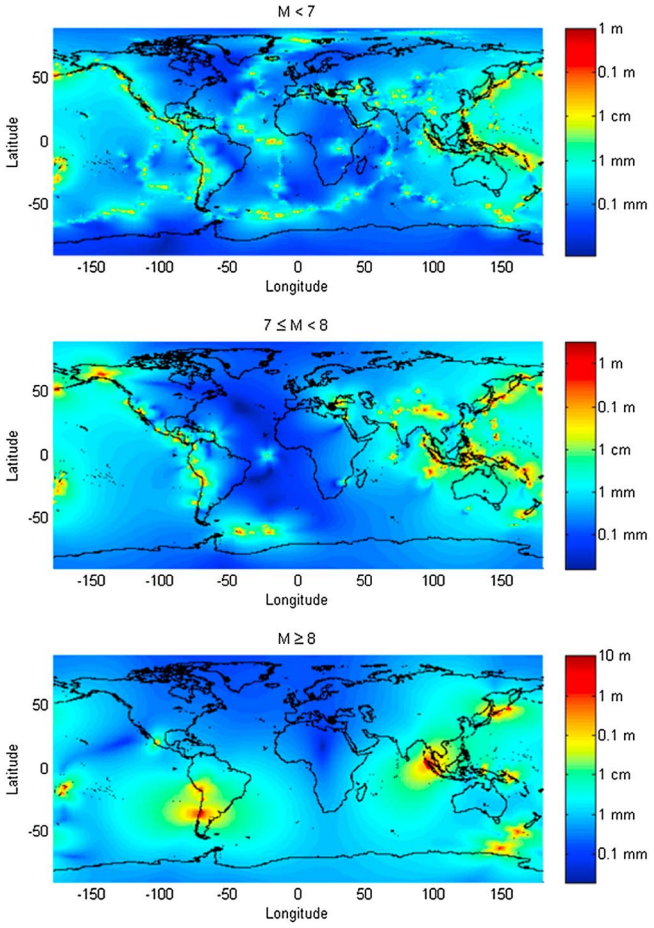

Figure 1. Theoretical cumulative coseismic ground displacement between 1 January 1991 and 31 December 2010 depending on the magnitude (*M*) range of EQ.

infer EQ-related discontinuities in GNSS (or other geodetic techniques) time series. The precision of hypocenter determinations may be an issue only for small EQs, and we will see in section 3 that the ratio of EQs with magnitude smaller than 7 that generate significant discontinuities in time series is very small. Finally, considering that the magnitude of coseismic deformations tends to zero away from the epicenter with a rate decreasing exponentially with the EQ magnitude, neglecting the Earth's sphericity may be an issue only for very large EQs. And for these EQs, the comparison between our results and the results from *Tregoning et al*. [2013], who used a method assuming a spherical Earth, show very similar solutions in magnitudes and patterns.

2.2. Theoretical Cumulative Coseismic Surface Deformation

Figure 1 shows the theoretical cumulative coseismic displacement from 1991 to 2010, calculated with our model, all over the world. The total displacement *U* for a given GPS station has been calculated as follows:

$$U = \sqrt{\left(\sum_i u_E^i\right)^2 + \left(\sum_i u_N^i\right)^2 + \left(\sum_i u_Z^i\right)^2} \quad (2)$$

where $u_E^i, u_N^i,$ and u_Z^i are, respectively, the east, north, and up components of the station coseismic displacement induced by the EQ number *i*. Note that for a given EQ, if we did not know which nodal plane did actually brake, we choose the nodal plane that produces the maximum displacement. Actually, we tested different rules for the nodal plane choice and we found that it does not change the presented map substantially. Indeed, for a given EQ, both nodal planes induce very similar deformations except in the close neighborhood of the epicenter. In section 3, we use a GPS network in which we observed that SAMP station (Sampali, Medan, Indonesia) was the only station sufficiently close to an epicenter (Sumatra–Andaman EQ in 2004) to induce a critical nodal plane choice. In order to limit this type of issue, the right fault nodal planes have been specified at least for the largest EQs, which have the advantage to be largely studied (notably EQs studied in Table 3) [e.g., *Freymueller et al*., 1994; *Fialko et al*., 2001; *Hreinsdottir et al*., 2003; *Fu and Sun*, 2006].

EQs with magnitude larger than 8 (Figure 1c) induce very large ground displacements, sometimes larger than 10 m with a wide geographical impact that can be at the centimeter level thousands of kilometers away from the epicenter [see also *Tregoning et al*., 2013]. However, we see that the accumulated displacements induced by smaller EQs can also be particularly large. Figure 1b shows the ground cumulative displacements induced by all EQs with magnitude between 7 and 8, whereas Figure 1a shows those induced by EQs with magnitude less than 7. We see that the cumulative displacements may be locally larger than 1 m in both cases but with different geographical patterns. As expected, displacements in extensive regions (e.g., close

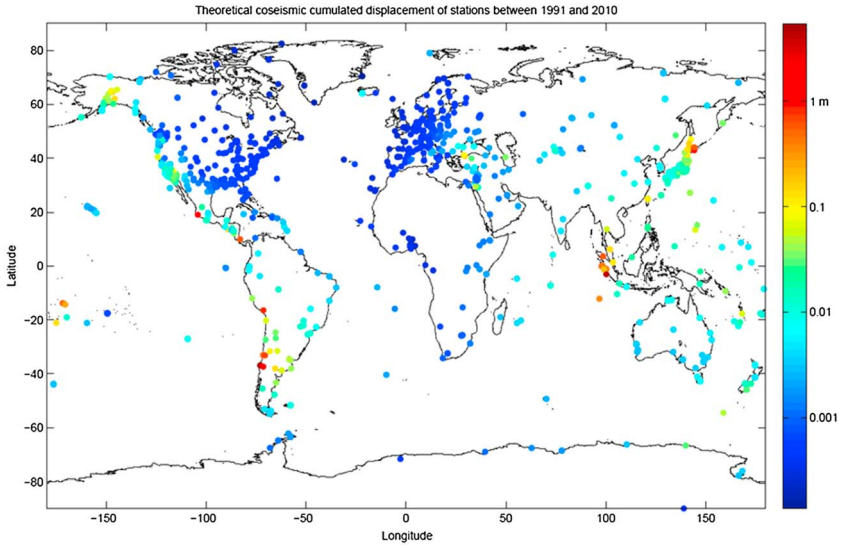

Figure 2. Theoretical cumulative coseismic motions of the GPS stations between 1 January 1991 and 31 December 2010.

to mid-oceanic ridges) are mostly induced by EQs smaller than 7, but the cumulative contribution of these EQs may be at the level of EQs with larger magnitude in the convergent regions (e.g., close to subduction zones). Note that in Figure 1c, the coseismic deformations from the largest EQs have been smoothed around the meridians that are 180° distant from epicenters in order to limit the visual impact of the error due to the half-space assumption. This error is negligible (at a level smaller than 0.1 mm) but is enhanced visually in the map due to the logarithmic scale.

We only investigate coseismic-accumulated deformations here. Postseismic deformations also induce additional deformations usually in the same direction as the coseismic offsets. In general, postseismic deformations remain far smaller than coseismic deformations. However, for mega earthquakes, *Trubienko et al*. [2014] showed that at a distance between 500 km to 1500 km to the epicenter, postseismic-accumulated deformations reach typically a value as large as the coseismic offset after 3–4 years of deformation. As a consequence, adding postseismic contributions may locally double the signal presented in Figure 1c.

3. Application on a GNSS Global Network: Handling Discontinuities

We investigate the impact of coseismic deformations on a global GPS solution. Our global GPS network is largely constituted of IGS network stations plus a few other stations. We used reprocessed combined GPS position time series as output of the first IGS reprocessing campaign (repro1) from 1997 to 2008. For the most recent data period (2008 to 2011), operational IGS solutions have been used. Station coordinates have been processed by the IGS as weighted averages of weekly station positions estimated using different software packages or parameterizations. For the first data period, we choose the recombined IGS repro1 solutions in order to ensure self-consistent time series over the whole period [*Rebischung et al*., 2012]. Apparent geocenter motion and rotational biases were removed following *Collilieux et al*. [2012] to derive the station position time series that we use. In total, the network contains 949 globally distributed stations (see Figure 2).

3.1. Cumulative Displacement

Figure 2 shows an interpolation of the global coseismic deformation on our GPS networks between 1991 and 2010 induced by all EQs with magnitude larger than 4. We see that a wide set of GPS stations may have accumulated more than a few meters motion due to successive seismic ruptures. This figure shows how a global GPS network will distort over time due to cumulative coseismic deformations, even from smaller EQs, and illustrates the importance of carefully taking into account coseismic discontinuities when one wants to construct a terrestrial reference frame.

Table 2. Discontinuities Detected in All the GPS Time Series[a]

	Initial Discontinuity Selection	New Discontinuity Selection
EQ discontinuity	235	439
Equipment discontinuity	364	362
Unknown discontinuity	264	231
Other discontinuity	44	41
Total number of discontinuity	907	1073

[a]In the "initial" case, the discontinuities have been selected classically; in the "new" case, the selection has been helped by our coseismic modeling. "Equipment discontinuity" stands for discontinuities due to equipment changes. "Other discontinuity" stands for discontinuities due to reasons other than equipment changes or EQs (e.g., firmware upgrade, local roadwork, and postseismicity treatment). "Unknown discontinuity" stands for discontinuities due to undetermined reasons.

3.2. Discontinuity Detection

The amplitude of EQ discontinuities is most of the time at the level of a few millimeters. For this reason, many EQ discontinuities may be missed in a visual inspection procedure. Thus, we would like to evaluate the importance of these undetected EQ discontinuities in position time series and reference frame analyses, particularly in the estimation of station velocities.

We conducted an experiment in which we compared global estimations of station velocities when discontinuities in GPS time series are detected classically, i.e., visually, and when discontinuities induced by coseismic deformations are determined from criteria based on our modeling approach. In the first approach, the list of discontinuity was based on IGS records and completed by our own direct visual observations. A comment is generally associated to the discontinuity when it is explained, such as the EQ name or magnitude when a correlation was observed between the epoch of an offset and the epoch of the event. The magnitude of the offset was tested with respect to a autoregressive (AR(1) type) background noise process in order to add only significant discontinuities [*Herring*, 2003; *Reilinger et al*., 2006]. In the second approach, we considered as relevant discontinuities those theoretical coseismic displacements with at least one component (east, north, or up component) larger than 2 mm in magnitude. The test has been made using the first model of EQ scaling statistics, i.e., the WC94 model. The threshold limit of 2 mm has been chosen empirically considering the general noise level of GPS station time series and the general consistency between the obtained new discontinuities and the actual time series. While this threshold limit may be relevant only for the present test, our aim here is only to illustrate how helpful a coseismic modeling approach can be, even a simple one, for EQ discontinuity detection, compared to what is classically done today. More sophisticated statistical tests may be investigated in the future for the development of generalized techniques for discontinuity detections in GPS time series.

Using the classical approach, for a total of 907 discontinuities referenced in GPS time series, 235 discontinuities were associated with EQ coseismic deformations (EQ discontinuities, see Table 2). When adding the list of discontinuities from the second approach, the number of discontinuities significantly increases. Indeed, 204 new EQ discontinuities were added for a total of 1073 discontinuities in the GPS time series (a 22% increase of the discontinuity number). We could also explain some of the visually detected discontinuities that were unexplained in our previous list of offsets. Nevertheless, a large number of unexplained discontinuities remain in the database and most of the new EQ discontinuities were actually new discontinuities. We note that in the initial set of discontinuities, a few were retrieved by our method with slight differences in their epochs. Figure 3a shows all stations, in our network, that are suspected to include an EQ discontinuity following our approach, grouped by EQ magnitude (M). Figure 3b presents a histogram of the number of EQ discontinuity versus the magnitude of the EQ that induced the discontinuities. Figure 3c presents a histogram of the number of EQs that are at the origin of EQ discontinuities in our GPS time series versus their magnitude. Only 103 EQs are responsible for all the EQ discontinuities during the period of observation. Sixty-five percent of these EQs have a magnitude greater than or equal to 7, but they are responsible for approximately 89% of all the EQ discontinuities. We see that EQs with magnitude smaller than 7 rarely induce significant discontinuities in our network GPS time series. Indeed, in Figure 3c, there are 33 EQs in the magnitude range of 6–7, which represents 2% of the EQs that occurred during this period in this magnitude range. Only two EQs can be found in the magnitude range of 5–6 (approximately 0.01% of the EQs that occurred in this magnitude range). On the contrary, only one EQ with magnitude greater than or equal to 8 did not generate a detectable EQ discontinuity in a GPS time series between 1998 and 2010. This EQ occurred in 2000 in the neighborhood of the Solomon Islands. All our GPS time series in this region actually begin after 2001, which explains why this EQ did not generate any discontinuity in our GPS time series.

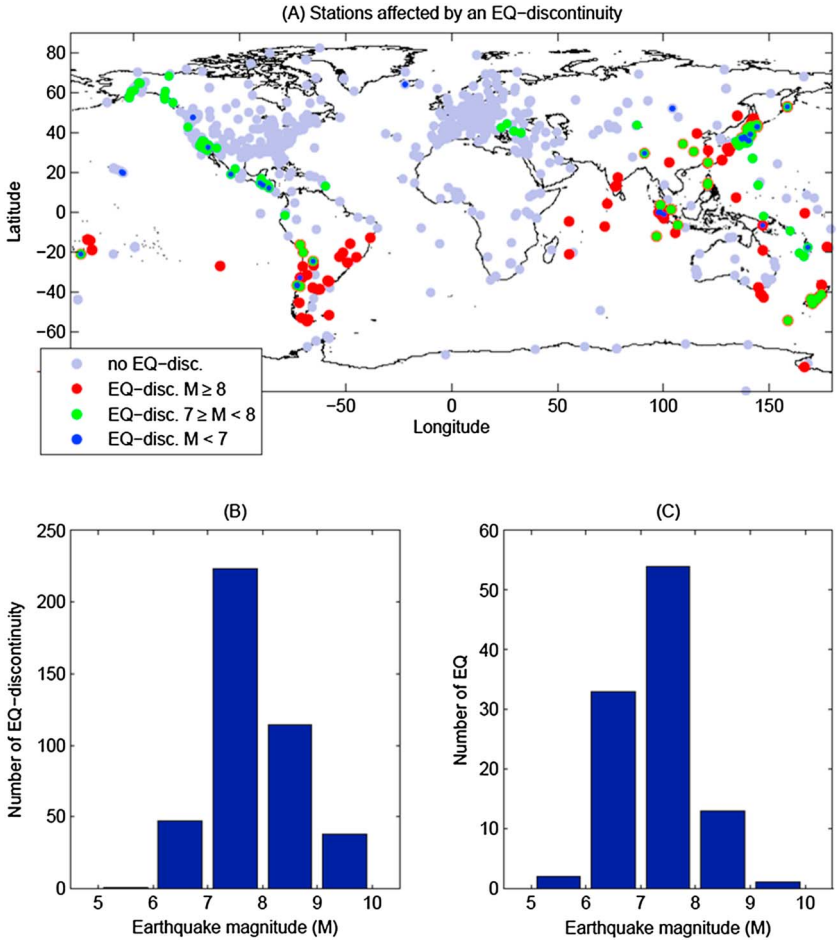

Figure 3. (a) Map of GPS stations that present an EQ discontinuity in their time series. (b) Total number of EQ discontinuities versus the magnitude of EQ. (c) Total number of EQ that induced an EQ discontinuity versus their magnitude.

In practice, the largest EQ discontinuities in our time series were already detected visually. Our approach is particularly interesting for the detection of smaller discontinuities that are, most of the time, clearly visible when one knows their existence but difficult to apprehend otherwise due to noise and seasonal variations. Figure 4 shows typical new EQ discontinuities detected in our GPS time series. From our experiment, we can distinguish between four types of situations in which a new EQ discontinuity may not be found without help from modeling:

1. A small discontinuity is clearly visible in the time series, but other large nonlinear components in the station time series make it minor or difficult to qualify as an EQ discontinuity, particularly if no large EQ occurred at this date (Figure 4, stations P106, WUHN, and SEAT).
2. The discontinuity is visible in the time series, but it can be confounded with natural variations, particularly when the time series present interannual variations or if there is not sufficient data before or after the EQ (Figure 4, stations SEAT, WUHN, and MOBS).
3. A discontinuity in position is not evident considering the seasonal variations and the measurement noise, but a clear change in velocity can be seen at the date of the EQ (Figure 4, stations AUCK and TOW2).
4. A discontinuity may be there, but it is not visible due to a lack of data in the time series (see Figure 6 and section 4.1)

Note the particular case of the Japanese station P106, whose time series presents two EQ discontinuities in 2003 that have not been detected using the classical protocol, because the operator would not expect that two EQs occurred during the same year and induced almost exact opposite displacements to the station. In such a case, the shifted points in the time series between the two EQ dates would typically be considered as outliers.

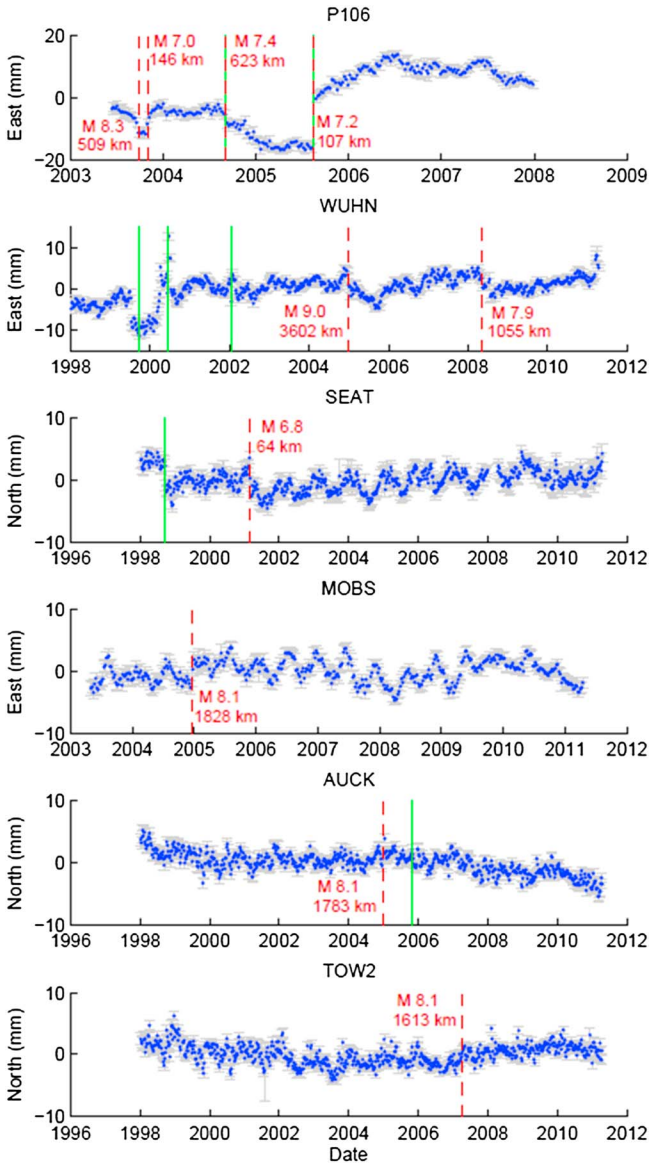

Figure 4. Examples of position time series from different GPS stations that present at least one EQ discontinuity detected using our approach (in red). The discontinuities that were already identified before using our approach are shown in green. These last ones are most of the time due to equipment changes, but some are also due to EQ (see P106 time series for instance).

To conclude, in all of these different situations, one would need help from an external theoretical indicator to identify the discontinuities in the time series. This is what motivates our approach.

A list of theoretical offsets for the GPS network that we investigated is provided as supporting information. The offsets in this list have been determined using the EQ scaling laws most adapted to each EQ (see section 4.2; we essentially used MB00 and YM11b models as a function of the EQ magnitude).

3.3. Impact on Velocities

We compared station velocities estimated using the two approaches discussed in section 3.2. For most of the stations, we constrained the velocity to be equal before and after the EQ discontinuity as it is classically done in geodetic time series analyses (we use the CATREF software for time series analyses, see *Altamimi et al.* [2002, 2007]). But some stations clearly show velocity changes after the discontinuity, for example, GPS stations subject to postseismic relaxation. In these particular cases, we did not constrain the velocity to be unique; therefore, these stations present distinct velocities at different time periods.

Figure 5 shows in color the maximum change in velocity that has been determined for each station. We see that many stations show velocity variations at the level of a few mm/yr, and in some extreme cases up to tens of mm/yr. Approximately 8% of the total number of stations present velocity variations larger than 1 mm/yr, 13% larger than 0.5 mm/yr, and 28% larger than 0.1 mm/yr. Note that Figure 5 does not show a particular spatial coherence. The reason is that the largest discontinuities were detected in both approaches. As a consequence, the velocity variations only concern stations that present in their time series small discontinuities that were initially missed.

4. Comparisons Between Models and Observations

4.1. Hector Mine Earthquake

As an example, we look more closely at the Hector Mine EQ (magnitude 7.1) that occurred in 1999 in the United States, in a region where the GPS station network is very dense. Figure 6 presents the theoretical coseismic ground motion that the region experienced. The ground motion shows a typical pattern associated with a strike dip rupture with coseismic displacements larger than 10 cm close to the epicenter. Note that

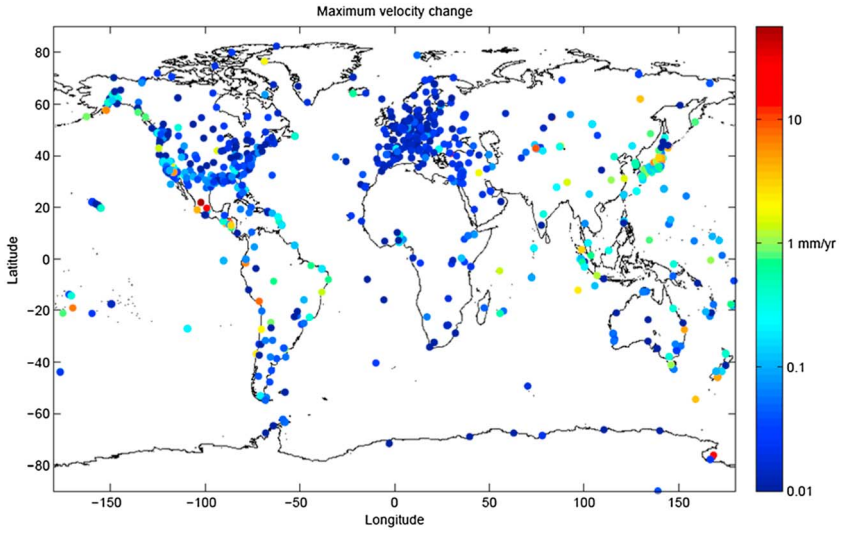

Figure 5. Maximum velocity changes of GPS stations induced by the addition of the new EQ discontinuities in the time series treatment.

in order to better see the pattern of the ground vertical motion, the colors have been saturated in the figure. Figure 7 presents the GPS station motions in the regions as estimated by the coseismic model (magenta arrows) and our time series analysis (white arrows). Here the EQ scaling model that has been used is the YM11b that appears here to be the most suited for the Hector Mine EQ (see Table 3 and section 4.2). Note that if YM11b is the model that works here the best, it does not mean that the fault geometry provided

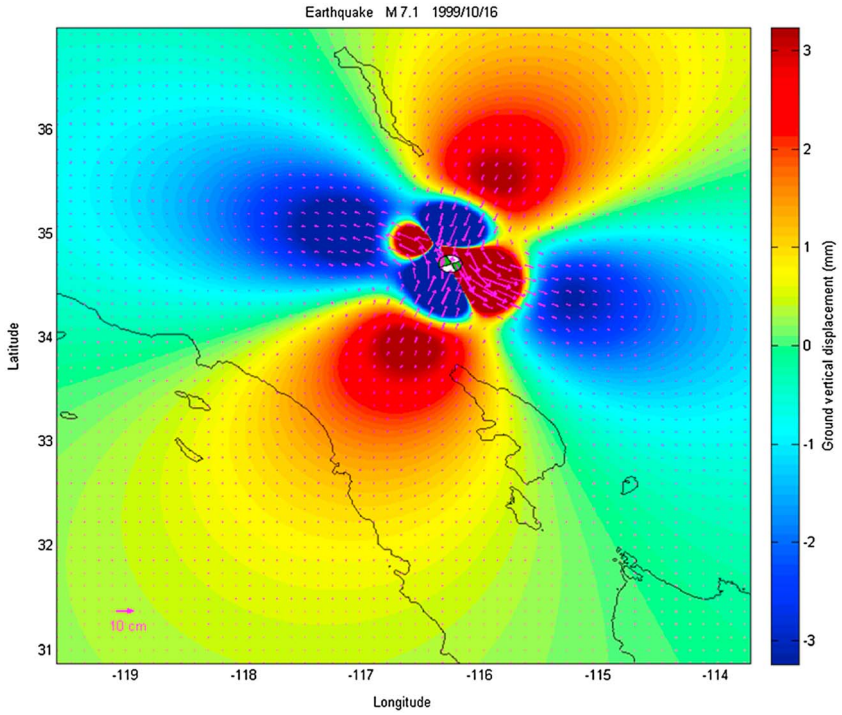

Figure 6. Theoretical ground motion induced by the Hector Mine Earthquake in 16 October 1999 calculated using the Okada approach [*Okada*, 1985]. In order to better see the pattern of the ground vertical motion, the colors have been saturated.

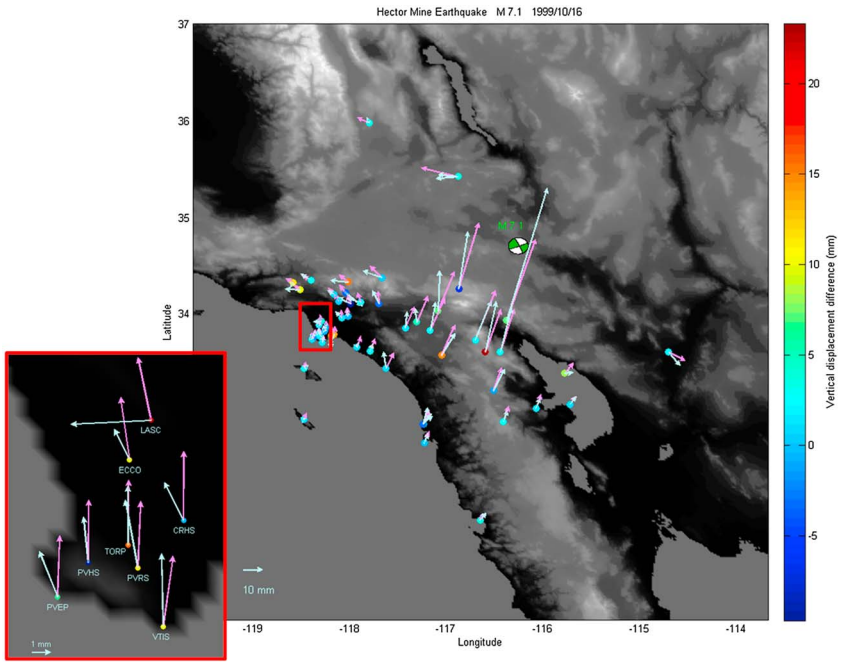

Figure 7. GPS station coseismic displacements induced by the Hector Mine EQ from our theoretical model (pink arrows based on YM11b scaling laws) and from the actual shift that we observe on GPS positions after the time series stacking using our discontinuity selection (white arrows). The differences between vertical velocities are shown in color. The red box shows a zoom on a few Los Angeles GPS stations.

by YM11b is the more realistic. Indeed, YM11b scaling laws assume square rupture faults with a very small mean slip. As mentioned by *Yen and Ma* [2011], these are effective geometrical parameters that have been used to better fit observations, not the real mean parameters that should be observed in the field. If we compare various published estimations of the Hector Mine EQ slip history [e.g., *Peltzer et al.*, 2001; *Ji et al.*, 2002; *Jacobs et al.*, 2002; *Simons et al.*, 2002; *Salichon et al.*, 2004], we see that the real geometrical characteristics of the fault are closer to those provided by WC94 scaling laws, which have been determined from ground or aftershock-related observations (see section 2.1 for more explanations), i.e., a mean fault length of 56 km, a mean fault width of 18 km, and a mean slip about 1.3 m (the maximum slip being typically 6 m locally on the fault [e.g., *Simons et al.*, 2002]).

In Figure 7, the arrows are only plotted for stations that present an EQ discontinuity (using the approach from section 3.2). The arrows from the model and the observations do not match exactly, but they are nevertheless quite close and show the same general coseismic pattern. Initially, only 26 discontinuities were detected

Table 3. Three-Dimensional RMS (in mm) of the Difference Between the GPS Estimated and the Theoretical Calculations of Coseismic Offsets for Different Earthquakes (EQs) and Depending on the EQ Scaling Model Used in the Coseismic Modeling[a]

EQ (*M*)	SU (9.0)	CH (8.8)	HO (8.3)	MA (8.1)	DE (7.9)	NZ (7.8)	HS (7.4)	BA (7.2)	HM (7.1)
GPS Stations	40	26	20	21	12	14	19	20	52
Scaling model									
WC94	26.0	530.8	125.2	4.80	11.16	19.90	4.0 4	6.29	5.74
MB00	**9.0**	**89.9**	**69.6**	5.02	13.57	**19.88**	4.25	6.51	5.71
BL10	19.0	167.5	115.5	**4.79**	10.84	19.94	3.98	6.44	5.23
ST10	49.7	180.1	98.3	4.87	**10.83**	19.95	3.88	6.50	5.37
YM11a	190.2	312.1	79.8	5.06	13.17	20.17	4.56	7.01	5.39
YM11b	21.8	358.5	90.8	4.88	11.08	19.92	**3.85**	**5.93**	**5.17**

[a]In bold: the smallest RMS for each EQ.

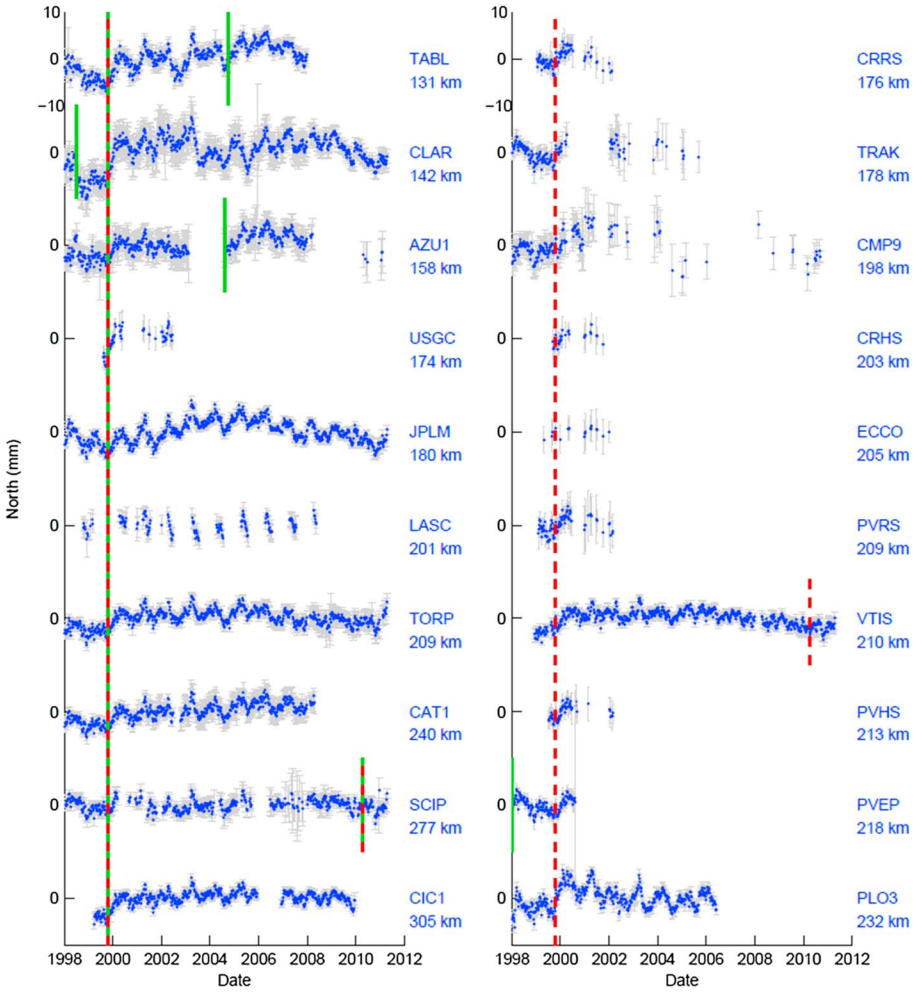

Figure 8. Examples of GPS position time series (north component) in the region surrounding the Hector Mine EQ epicenter (1999). The distance between the GPS station and the hypocenter is indicated under each station code. These time series do not present large shift at the time of the EQ, but they show a global mean shift of a few millimeters before and after the EQ date. The indicated EQ discontinuities that have been identified by our method are shown in red, and all the discontinuities that were already identified before using our approach (due to equipment changes and/or EQ) are shown in green.

in the station time series; after our treatment, the number increased to 50. A few stations close to the epicenter do not show arrows because their time series actually begin after the date of the Hector Mine EQ. A few station time series present very clear discontinuities at the date of the EQ, particularly on the north component position time series. However, it can be noted that many stations, particularly on the northwestern part of the region, do not show a clear instantaneous discontinuity, while the whole time series shows a global mean shift of a few millimeters before and after the EQ date (see Figure 8). It means that the discontinuity in these station time series is partially hidden by data noise and can be easily missed visually, particularly if the time series do not present sufficient points (as for stations in Figure 8 (right)). Yet neglecting this discontinuity in these time series would be problematic for the estimation of station velocities.

Note that the weekly average of GPS station positions may also hide an instantaneous coseismic offset if the later occurred in the middle of the week. This could make the visual detection of small offsets even more difficult and may explain, in Figure 7, that the observed offsets are most of the time slightly smaller than the theoretical ones.

4.2. GNSS Constraint on EQ Scaling Statistics

If coseismic modeling helps to detect EQ discontinuities in GPS time series, our observations may in return give information on the quality or the relevance of the different scaling laws that have been used in our

study. Table 3 shows the root-mean-square (RMS) calculation of the difference between modeled and estimated coseismic 3-D displacements on the GPS stations for different selected EQs that impacted at least 12 stations (in our experiment in section 3.2). Ordered by decreasing magnitude, the investigated EQs are Sumatra EQ in 2004 (SU), Chile EQ in 2010 (CH), Hokkaido EQ in 2003 (HO), Macquarie EQ in 2004 (MA), Denali EQ in 2002 (DE), New Zealand EQ in 2009 (NZ), Honshu EQ in 2004 (HS), Baja EQ in 2010 (BA), and Hector Mine EQ in 1999 (HM). The absolute values of the RMS, as well as comparisons between the different EQs in terms of RMS value, are meaningless because the EQ did not affect the same number of stations with the same magnitude and with the same local network configuration. However, for each EQ, we can determine which scaling laws tend to better reproduce our GPS measurements, i.e., which gives the smaller RMS (in bold in Table 3). The global answer is at first sight obscured because the preferred scaling laws vary strongly with the EQ. However, despite small differences, one can see a general tendency that seems to depend on the magnitude of the EQ. We see that the classical WC94 is not the best model here for EQ source calibration. One may distinguish three distinct groups depending on the EQ magnitude. For great EQs with magnitude larger than 8.1–8.2, the preferred scaling laws are those presented by MB00. For smaller magnitudes, particularly in the magnitude range of 7.4 to 8.1, there is no clear preferred model. Three different EQs give three different preferred scaling laws between the ST10, BL10, and MB00 models. But the RMS given by all the scaling law models are relatively close to each other. For smaller magnitude EQs, the preferred scaling laws are always those from YM11b. As a consequence, the ideal EQ scaling law statistics for an Okada approach might be a combination of the different published statistics depending on the magnitude of EQ (see the next section for discussions).

5. Discussions and Conclusions

We investigated theoretical coseismic deformations at global scale during approximately two decades. It appears that the accumulated coseismic displacements can be very large and that almost no region in the world is spared.

As shown by *Tregoning et al*. [2013], EQs with magnitude larger than 8 induce ground displacements sometimes larger than 10 m, with a geographical extent that can be thousands of kilometers away from the epicenter (for a displacement at the centimeter level). However, we see that the accumulated displacements induced by smaller EQs can also be particularly large, up to a few meters, with different geographical patterns than greater EQs. Considering the current precision in geodetic techniques, we see that 20 years of coseismic motions have a wide impact on the Earth's surface. In particular, the accumulation of large but also very small motions leads to large visible cumulative displacements not only in the neighborhood of giant EQs. *Tregoning et al*. [2013] concluded that Australia and North Atlantic/Arctic ocean regions did not undergo significant deformation due to great EQs during a decade. We show here that these regions did undergo cumulative coseismic deformations, during the same period due to smaller EQs, that may be locally at the centimeter to meter level.

We then showed that a global modeling of coseismic deformations helps to detect discontinuities in GPS time series. We conducted an experiment in which we estimated GPS station positions and velocities on a global network with or without the help of discontinuity detection from a simple coseismic model. We see that the approach with coseismic modeling significantly increases the number of detected discontinuities in the GPS time series, almost doubling the detected EQ discontinuities in our case. It suggests that numerous EQ discontinuities are too small to be visually qualified because seasonal variations and GPS noise perturb the identification. However, not taking the discontinuity into account may have a strong impact on the station velocity estimation. As a consequence, if we want to gain an order of magnitude in the precision of estimated geodetic station positions and velocities, we cannot rely anymore on visual assumptions only. We need to develop techniques based on numerical criteria to detect the presence of discontinuities in time series using all types of external information including geophysical information. A limitation in our modeling approach is that the detection of a discontinuity depends on an arbitrary threshold value in coseismic displacement, which highly depends on the EQ scaling model that we use. A way to overcome this point might be to combine geophysical modeling with statistical methods for automatic discontinuity detection in time series [*Williams*, 2003; *Perfetti*, 2006; *Vitti*, 2012; *Gazeaux et al*., 2013]. As a by-product of our work, we plan to set up a Web service that will provide coseismic offsets on demand for a list of stations that would be given by the user. Users would then freely define their own criteria to decide whether a coseismic offset would induce a discontinuity in

a GPS time series or not. The information could also be used as a priori information in automated methods for discontinuity detection. For the time being, we provide, as supporting informaton, a list of theoretical offsets for the GPS network that we investigated here.

Note that in our approach, we suppose that coseismic stresses are fully transferred across plate boundaries. Yet one may expect stress changes to only propagate across locked plate boundaries. However, this issue, which would affect the coseismic deformation pattern, is not straightforward to address here. Indeed, if we can expect mid-oceanic ridges to be unlocked, the question is far more complex for subduction zones and strike-slip faults, where it would depend on local tectonic configurations. Moreover, observations tend to comfort the approach that we used even across mid-oceanic ridges. For instance, if no stress was able to propagate beyond the Indian mid-oceanic ridge, then stations like REUN should not have any discontinuity induced by the Sumatra–Andaman EQ, yet a small discontinuity may be visible in REUN time series at that date (see Figure S1 in the supporting information). We therefore prefer assuming full stress transfer and leave this fundamental issue, which goes beyond the scope of the paper, for dedicated studies.

We then compared the predicted coseismic displacements to the estimated offsets in GPS time series. As an example, we look at the Hector Mine EQ. The EQ has been recorded in many stations due to a local dense GPS network. But many EQ discontinuities had not been detected in the time series because the instantaneous seismic shift was sometimes small, sometimes invisible due to a lack of data. Yet neglecting these discontinuities would be problematic in the estimation of station velocities. Indeed, even if the instantaneous seismic offset is sometimes not visible, all the time series show the same tendency with a general shift between the time series before and after the EQ.

Finally, we studied the EQ scaling laws with respect to global GPS observations. We investigated nine EQs whose coseismic deformations were recorded by at least 12 stations and calculated RMS between recorded and calculated offsets in time series. We see that for great EQs with magnitude larger than 8.1–8.2, the preferred scaling laws are those presented by MB00. For smaller magnitudes, particularly in the magnitude range of 7.4 to 8.1, there is no clear preferred model. Three different EQs give three different preferred scaling laws, between ST10, BL10, and MB00 models. For even smaller magnitudes, despite small differences, the preferred scaling laws are always those from YM11b. Note that this last model is in reality composed of two groups of scaling laws, one dedicated for EQs with moment magnitude larger than 10^{20} Nm (EQ magnitude approximately equal to 7.3) and the other for EQs with moment magnitude smaller. This means that the good consistency between our GPS observations and the coseismic modeling is only for the second group of scaling laws in which the effective fault plane is assumed to be square. We see also that the classical WC94 is not the best model here for representing the EQ source. Its performance remains equivalent to the other models in the range of magnitudes 7.4 to 8.1. The results that we obtain do not mean that WC94 statistics give wrong mean fault geometries; it only shows that MB00 and YM11b are particularly well adapted here. It may be logical because these two statistics are inferred from finite fault rupture models. These models propose effective fault parameters that fit surface deformations and geodetic observations, assuming faults and rupture slips, whatever their complexity, in an infinite half elastic medium as in the Okada approach for coseismic deformations. Therefore, the statistics proposed by MB00 and YM11b may lead to effective fault geometries that are not consistent with what is really observed in the field but that give the most consistent results in terms of surface deformations when using an Okada model for coseismic deformations. To conclude, we show that the EQ scaling law statistics based on finite fault rupture models are better adapted for an Okada approach, and among those statistics, the choice of a preferred one tends to depend on the magnitude of the EQ.

Acknowledgments

We thank Matt King and Jeff Freymueller for their careful reviews of our work and the Editor Paul Tregoning. We use a USGS National Earthquake Information Center (NEIC) catalog of seismicity and information from the global Centroid Moment Tensor (CMT) catalog for earthquake source parameters. The earthquake source database can be downloaded at www.globalcmt.org website (http://www.globalcmt.org/CMTfiles.html). The Okada coseismic code that we used is available at the address www.ipgp.fr/~beaudu/. Finally, the GPS data are available through the International GNSS service (IGS) website at the address http://webigs.ign.fr/en/. We thank Centre National d'Etudes Spatiales for financial support through the TOSCA committee. This work is IPGP contribution number 3586.

References

Aki, K., and P. G. Richards (1980), *Quantitative Seismology*, Freemann & Co., New York.

Altamimi, Z., P. Sillard, and C. Boucher (2002), ITRF2000: A new release of the International Terrestrial Reference Frame for Earth science applications, *J. Geophys. Res.*, *107*(B10), 2214, doi:10.1029/2001JB000561.

Altamimi, Z., X. Collilieux, J. Legrand, B. Garayt, and C. Boucher (2007), ITRF2005: A new release of the International Terrestrial Reference Frame based on time series of station positions and Earth orientation parameters, *J. Geophys. Res.*, *112*, B09401, doi:10.1029/2007JB004949.

Altamimi, Z., X. Collilieux, and L. Métivier (2011), ITRF2008: An improved solution of the International Terrestrial Reference Frame, *J. Geod.*, *85*(8), 457–473, doi:10.1007/s00190-011-0444-4.

Altamimi, Z., L. Métivier, and X. Collilieux (2012), ITRF2008 Plate Motion Model, *J. Geophys. Res.*, *117*, B07402, doi:10.1029/2011JB008930.

Blaser, L., F. Krüger, M. Ohmberger, and F. Scherbaum (2010), Scaling relations of earthquake source parameter estimates with special focus on subduction environment, *Bull. Seismol. Soc. Am.*, *100*(6), 2914–2926, doi:10.1785/0120100111.

Collilieux, X., Z. Altamimi, D. Coulot, J. Ray, and P. Sillard (2007), Comparison of VLBI, GPS, SLR height residuals from ITRF2005 using spectral and correlation methods, *J. Geophys. Res.*, *112*, B12403, doi:10.1029/2007JB004933.

Collilieux, X., T. van Dam, J. Ray, D. Coulot, L. Métivier, and Z. Altamimi (2012), Strategies to mitigate aliasing of loading signals while estimating GPS frame parameters, *J. Geod.*, *86*, 1–14, doi:10.1007/s00190-011-0487-6.

Dong, D., P. Fang, Y. Bock, M. Cheng, and S. Miyazaki (2002), Anatomy of apparent seasonal variations from GPS-derived site position time series, *J. Geophys. Res.*, *107*(B4), 2075, doi:10.1029/2001JB000573.

Dziewonski, A. M., T.-A. Chou, and J. H. Woodhouse (1981), Determination of earthquake source parameters from waveform data for studies of global and regional seismicity, *J. Geophys. Res.*, *86*, 2825–2852, doi:10.1029/JB086iB04p02825.

Ekström, G., M. Nettles, and A. M. Dziewonski (2012), The global CMT project 2004-2010: Centroid-moment tensors for 13,017 earthquakes, *Phys. Earth Planet. Inter.*, *200-201*, 1–9, doi:10.1016/j.pepi.2012.04.002.

Fialko, Y., M. Simmons, and D. Agnew (2001), The complete (3-D) surface displacement field in the epicentral area of the 1999 Mw 7.1 Hector Mine earthquake California from space geodetic, *Geophys. Res. Lett.*, *28*(16), 3063–3066, doi:10.1029/2001GL013174.

Freymueller, J., N. E. King, and P. Segall (1994), The co-seismic slip distribution of the landers earthquake, *Bull. Seismol. Soc. Am.*, *84*(3), 646–659.

Fu, G., and W. Sun (2006), Global co-seismic displacements caused by 2004 Sumatra-Andaman earthquake (Mw 9.1), *Earth Planets Space*, *58*, 149–152.

Gazeaux, J., et al. (2013), Detecting offsets in GPS time series: First results from the detection of offsets in GPS experiment, *J. Geophys. Res. Solid Earth*, *118*, 2397–2407, doi:10.1002/jgrb.50152.

Herring, T. (2003), MATLAB Tools for viewing GPS velocities and time series, *GPS Solutions*, *7*, 194–199, doi:10.1007/s10291-003-0068-0.

Hreinsdottir, S., J. T. Freymueller, H. J. Fletcher, C. F. Larsen, and R. Bürgmann (2003), Coseismic slip distribution of the 2002 MW 7.9 Denali fault earthquake, Alaska, determined from GPS measurements, *Geophys. Res. Lett.*, *30*(13), 1670, doi:10.1029/2003GL017447.

Jacobs, A., D. Sandwell, Y. Fialko, and L. Sichoix (2002), The 1999 (Mw =7.1) Hector Mine, California earthquake: Near-field post seismic deformation from ERS interferometry, *Bull. Seismol. Soc. Am.*, *92*(4), 1433–1442.

Ji, C., J. D. Wald, and D. V. Helmberger (2002), Source description of the 1999 Hector Mine, California earthquake. II. Complexity of slip history, *Bull. Seismol. Soc. Am.*, *92*(4), 1208–1226.

Kreemer, C., G. Blewitt, W. C. Hammond, and H.-P. Plag (2006), Global deformation from the great 2004 Sumatra-Andaman Earthquake observed by GPS: Implications for rupture process and global reference frame, *Earth Planets Space*, *58*, 141–148.

Mai, M., and G. C. Beroza (2000), Source scaling properties from finite-fault-rupture models, *Bull. Seismol. Soc. Am.*, *90*(3), 604–615.

Métivier, L., and C. P. Conrad (2008), Body tides of a convecting, laterally heterogeneous, and aspherical Earth, *J. Geophys. Res.*, *113*, B11405, doi:10.1029/2007JB005448.

Métivier, L., M. Greff-Lefftz, and M. Diament (2005), A new approach to compute accurate gravity time variations for a realistic Earth model with lateral heterogeneities, *Geophys. J. Int.*, *162*, 570–574.

Métivier, L., M. Greff-Lefftz, and M. Diament (2006), Mantle lateral variations and elasto-gravitational deformations - I. Numerical modeling, *Geophys. J. Int.*, *167*, 1060–1076, doi:10.1111/j.1365-246X.2006.03159.x.

Métivier, L., M. Greff-Lefftz, and M. Diament (2007), Mantle lateral variations and elasto-gravitational deformations - II. Possible effects of a superplume on body tides, *Geophys. J. Int.*, *168*, 897–903, doi:10.1111/j.1365-246X.2006.03309.x.

Métivier, L., X. Collilieux, and Z. Altamimi (2012), ITRF2008 contribution to glacial isostatic adjustment and recent ice melting assessment, *Geophys. Res. Lett.*, *39*, L01309, doi:10.1029/2011GL049942.

Murotani, S., H. Miyake, and K. Koketsu (2008), Scaling of characterized slip models for plate-boundary earthquakes, *Earth Planets Space*, *60*, 987–991.

Okada, Y. (1985), Surface deformation due to shear and tensile faults in a half-space, *Bull. Seismol. Soc. Am.*, *75*(4), 1135–1154.

Peltzer, G., F. Crampé, and P. Rosen (2001), The Mw 7.1, Hector Mine, California earthquake: Surface rupture, surface displacement field and fault slip solution from ERS SAR data, *C. R. Acad. Sci. Paris*, *333*, 545–555.

Perfetti, N. (2006), Detection of station coordinate discontinuities within the Italian GPS Fiducial Network, *J. Geod.*, *80*, 381–396, doi:10.1007/s00190-006-0080-6.

Plag, H.-P., and M. Pearlman (2009), *The Global Geodetic Observing System: Meeting the Requirements of a Global Society on a Changing Planet in 2020*, Springer, Berlin, Germany.

Ray, J., Z. Altamimi, X. Collilieux, and T. van Dam (2008), Anomalous harmonics in the spectra of GPS position estimates, *GPS Solutions*, *12*(1), 55–64, doi:10.1007/s10291-007-0067-7.

Rebischung, P., B. Garayt, X. Collilieux, and Z. Altamimi (2012), IGS Reference Frame Working Group Coordinator Report 2011, IGS Tech. Rep., 2011, Astronomical Institute of the Univ. of Bern.

Reilinger, R. S., et al. (2006), GPS constraints on continental deformation in the Africa-Arabia-Eurasia continental collision zone and implications for the dynamics of plate interactions, *J. Geophys. Res.*, *111*, B05411, doi:10.1029/2005JB004051.

Romanowicz, B., and L. J. Ruff (2002), On moment-length scaling of large strike slip earthquakes and the strength of faults, *Geophys. Res. Lett.*, *29*(12), 1604, doi:10.1029/2001GL014479.

Salichon, J., P. Lundgren, B. Delouis, and D. Giardini (2004), Slip history of the 16 October 1999 M_w 7.1 Hector Mine Earthquake (California) from the inversion of InSAR, GPS and Teleseismic data, *Bull. Seismol. Soc. Am.*, *94*(6), 2015–2027.

Scholz, C. H. (1990), *The Mechanics of Earthquakes and Faulting*, Cambridge Univ. Press, Cambridge, U. K.

Shestakov, N. V., et al. (2012), Analysis of the far-field crustal displacements caused by the 2011 Great Tohoku earthquake inferred from continuous GPS observations, *Tectonophysics*, *524–525*, 76–86, doi:10.1016/j.tecto.2011.12.019.

Simons, M., Y. Fialko, and L. Rivera (2002), Coseismic deformation from the 1999, Mw =7.1, Hector Mine earthquake as inferred from InSAR and GPS observations, *Bull. Seismol. Soc. Am.*, *92*(4), 1390–1402.

Strasser, F. O., M. C. Arango, and J. J. Bommer (2010), Scaling of the source dimensions of Interface and Intraslab Subduction-zone Earthquakes with moment magnitude, *Seismol. Res. Lett.*, *81*(6), 941–950, doi:10.1785/gssrl.81.6.941.

Subarya, C., M. Chlieh, L. Prawirodirdjo, J.-P. Avouac, Y. Bock, K. Sieh, A. J. Meltzner, D. H. Natawidjaja, and R. McCaffrey (2006), Plate-boundary deformation associated with the great Sumatra–Andaman earthquake, *Nature*, *440*, 46–51, doi:10.1038/nature04522.

Tregoning, P., R. Burgette, S. C. McClusky, S. Lejeune, C. S. Watson, and H. McQueen (2013), A decade of horizontal deformation from great earthquakes, *J. Geophys. Res. Atmos.*, *118*, 2371–2381, doi:10.1002/jgrb.50154.

Trubienko, O., J.-D. Garaud, and L. Fleitout (2014), Models of postseismic deformation after megaearthquakes: The role of various rheological and geometrical parameters of the subduction zone, *Solid Earth Discuss.*, *6*, 427–466, doi:10.5194/sed-6-427-2014.

Vigny, C., et al. (2005), Insight into the 2004 Sumatra-Andaman earthquake from GPS measurements in southeast Asia, *Nature*, *436*, 201–206, doi:10.1038/nature03937.

Vitti, A. (2012), SIGSEG: A tool for the detection of position and velocity discontinuities in geodetic time-series, *GPS Solutions*, *16*, 405–410, doi:10.1007/s10291-012-0257-9.

Wells, D. L., and K. J. Coppersmith (1994), New empirical relationships among magnitude, rupture length, rupture width, rupture area and surface displacement, *Bull. Seismol. Soc. Am.*, *84*(4), 974–1002.

Williams, S. D. P. (2003), Offsets in global positioning system time series, *J. Geophys. Res.*, *108*(B6), 2310, doi:10.1029/2002JB002156.

Yen, Y.-T., and K.-F. Ma (2011), Source-scaling relationship for M 4.6–8.9 earthquakes, specifically for earthquakes in the collision zone of Taiwan, *Bull. Seismol. Soc. Am.*, *101*(2), 464–481, doi:10.1785/0120100046.